Proc. Natl. Acad. Sci. USA
Vol. 95, pp. 11555–11560, September 1998
Biochemistry

RNA folding causes secondary structure rearrangement

MING WU AND IGNACIO TINOCO, JR.†

Department of Chemistry, University of California, Berkeley, and Structural Biology Department, Lawrence Berkeley National Laboratory, Berkeley, CA 94720-1460

Contributed by Ignacio Tinoco, Jr., July 21, 1998

ABSTRACT **The secondary structure of the P5abc subdomain (a 56-nt RNA) of the *Tetrahymena thermophila* group I intron ribozyme has been determined by NMR. Its base pairing in aqueous solution in the absence of magnesium ions is significantly different from the RNA in a crystal but is consistent with thermodynamic predictions. On addition of magnesium ions, the RNA folds into a tertiary structure with greatly changed base pairing consistent with the crystal structure: three Watson–Crick base pairs, three G·U base pairs, and an extra-stable tetraloop are lost. The common assumption that RNA folds by first forming secondary structure and then forming tertiary interactions from the unpaired bases is not always correct.**

RNA plays many roles in biological processes, and our knowledge of its importance is still expanding rapidly (1, 2). By understanding how RNA folds into its three-dimensional structure, we can begin to predict its folding from its sequence and can greatly improve our understanding of its biological functions. The standard RNA folding mechanism is a two-step process. The RNA first folds into a secondary structure, which then folds into a three-dimensional tertiary structure stabilized by interactions between the preformed secondary structural motifs (3–7). Divalent metal ions bound at a few specific locations appear to be crucial for the tertiary folding (8, 9). RNA secondary structures can be deduced from a phylogenetic comparison of many related sequences or from a calculation of free energies (based on thermodynamic measurements of model oligonucleotides) for stable secondary structures. Secondary structures and low-resolution tertiary structures can also be obtained from biochemical experiments that reveal nucleotide accessibility and detect long-range interactions. However, NMR spectroscopy and x-ray diffraction are the major tools for high-resolution structure determination of RNA.

The crystal structure of the P4–P6 domain of the *Tetrahymena* group I intron at high resolution (10–12) has revealed a tremendous amount of new information on RNA structure and folding. When the *Tetrahymena* group I intron (414 nt) folds into a catalytically active form, the 160-nt P4–P6 domain is the first to fold (6, 13, 14). Cleavage experiments with Fe-EDTA showed that the isolated domain and the domain in the intron fold into the same tertiary structure on addition of millimolar concentrations of magnesium ions (15). A cluster of five Mg^{2+} were found coordinated to phosphate oxygen atoms in the A-rich bulge and in the 3-helix junction of the P5abc subdomain of the P4–P6 domain (10, 11). To confirm the identities of the metal-coordinated phosphate groups, phosphorothioate substitution experiments were performed on the 160-nt P4–P6 domain and a 56-nt P5abc subdomain (9). Native gel electrophoresis experiments separated two forms of the RNA molecules: folded and unfolded. By systematically replacing sulfur atoms for oxygen atoms, seven pro-Rp phosphate oxygens were found to be necessary for tertiary folding in solution in both the P4–P6 domain and its P5abc subdomain. Except for one substitution that disrupts an RNA–RNA hydrogen bond, all sites involve magnesium ion coordination to the same phosphate groups identified in the crystal structure. These results support the hypothesis that RNA folds on a magnesium ion core (9) and also suggest that the P5abc subdomain folds the same as the P4–P6 domain.

In this work, we determined the secondary structure of the 56-nt P5abc subdomain RNA in the absence of magnesium ions and found that this secondary structure is significantly different from the x-ray secondary structure (10). Magnesium-induced tertiary folding of P5abc changes the secondary structure to one that is consistent with x-ray structure. Our results contradict the usual assumption that RNA folds by first forming a secondary structure and then forming tertiary interactions from the unpaired bases.

METHODS

RNA Synthesis and Purification. All of the RNAs were enzymatically synthesized *in vitro* by using T7 RNA polymerase and chemically synthesized DNA templates (16, 17). RNAs were purified by using denaturing PAGE. We did not separate the desired 56-nt P5abc species from the N+1 species. This 3′ end inhomogeneity does not affect the structure, but it does cause doubling of the imino resonances of the last three base pairs. After gel purification, the RNA samples were dialyzed against the NMR buffer for 48 h. The samples were dried by using a SpeedVac (Savant Instruments, Hicksville, NY), resuspended in 90% H_2O/10% ^2H_2O, and transferred to NMR tubes for data acquisition.

NMR Spectroscopy. All spectra were acquired on a Bruker AMX-600 spectrometer (Billerica, MA); the data were processed by using FELIX software (Biosym Technologies, San Diego). One-dimensional (1D) and two-dimensional (2D) exchangeable proton spectra were acquired by using a 1-1 sequence for water suppression (18, 19).

Secondary Structure Determination by NMR. The 56-nt P5abc subdomain whose sequence is shown in Fig. 1*a* was dialyzed against a 10 mM sodium phosphate buffer (pH 6.4) for 48 h, lyophilized, and resuspended in 90% H_2O/10% ^2H_2O in a 5-mm Shigemi tube for NMR measurements. The imino proton resonances are exceptionally sharp, indicating that P5abc is in a single conformation with no aggregation that would broaden the peaks. UV melting indicates that P5abc forms a monomeric species in the micromolar to millimolar concentration range. The imino protons of guanine and uracil give rise to NMR peaks in the range of 10–15 ppm. In a 2D nuclear Overhauser effect (NOE) spectroscopy (NOESY) spectrum (Fig. 1*b*, *Lower*), the diagonal peaks match the imino

The publication costs of this article were defrayed in part by page charge payment. This article must therefore be hereby marked "*advertisement*" in accordance with 18 U.S.C. §1734 solely to indicate this fact.

Abbreviations: 1D, one-dimensional, 2D, two-dimensional, NOE, nuclear Overhauser effect; NOESY, NOE spectroscopy.

A Commentary on this article begins on page 11506.

†To whom reprint requests should be addressed. e-mail: intinoco@lbl.gov.

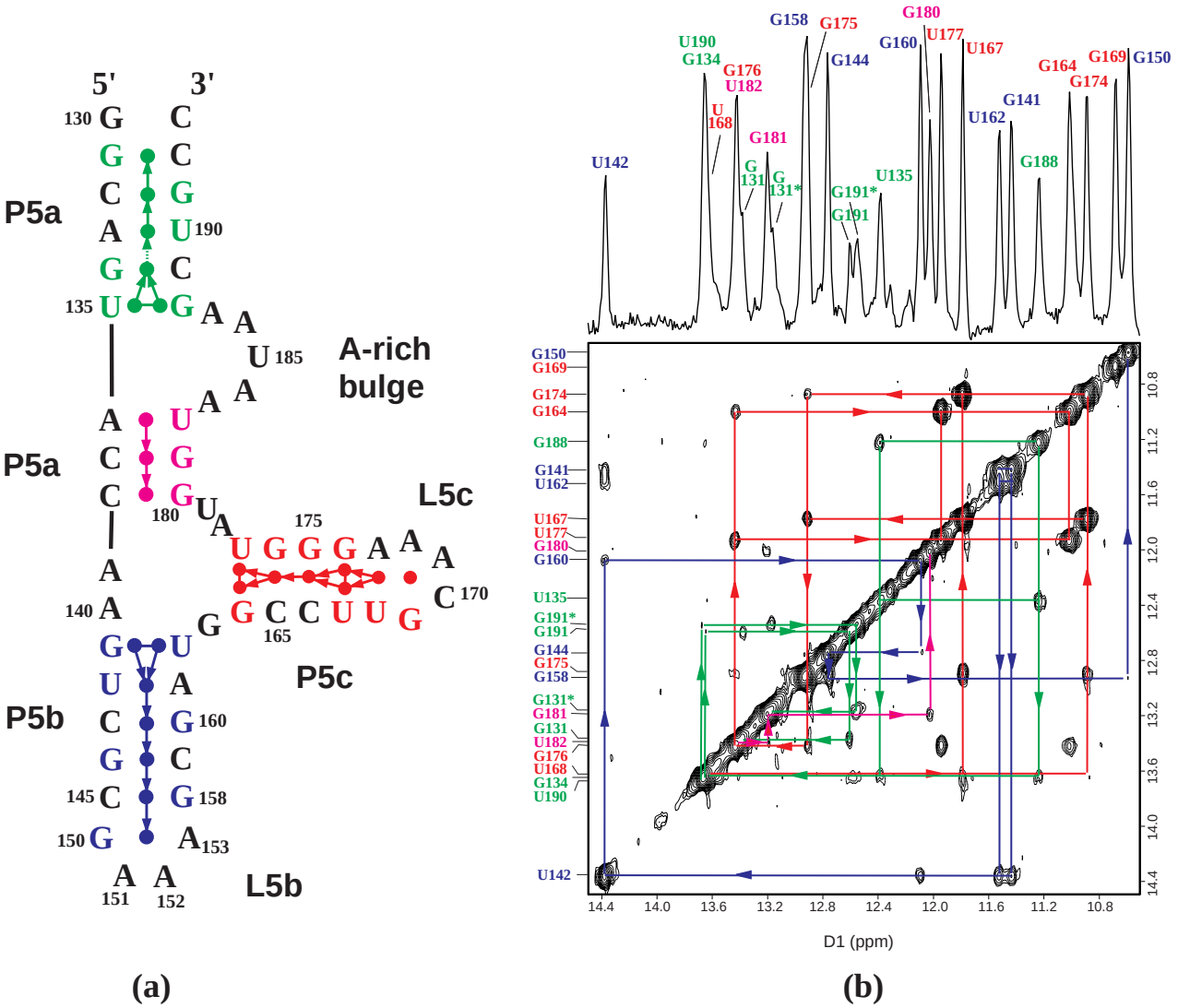

FIG. 1. (*a*) The secondary structure of the 56-nt P5abc subdomain. The numbering is the same as in the P4–P6 domain. P5abc has 4 bp deleted from the P4–P6 domain between the C145·G158 base pair of P5b and the L5b tetraloop GAAA (nucleotides 150–153); the 4-bp deletion causes the discontinuity in the numbering of this region. The disk between each base pair represents the observed imino proton of the base pair. The terminal G130 imino proton resonance is not observed by NMR because of the fraying of the G130·C193 base pair. Each arrow represents an NOE connectivity between two imino protons; the direction and color of the arrows match those of NOE walks in the 2D spectrum shown in *b*. The dotted arrow between the G134 and U190 imino protons indicates our inability to see the NOE between them caused by the near identity of their chemical shifts. (*b*) The 1D imino proton spectrum (*Upper*) and 2D 120-ms NOESY spectrum (*Lower*) of 2.5 mM of P5abc in 10 mM sodium phosphate and 0.01 mM EDTA (pH 6.4) in 90% H_2O/10% ^2H_2O at 10°C. The 1D spectrum was acquired with 4K complex points and processed with a 25°-shifted sine bell squared window function. The 2D data were acquired with 4K points in the D1 dimension and 512 points in the D2 dimension, and were processed with a 40°-shifted sine bell squared function. The arrows connecting diagonal peaks and crosspeaks and the NOE connectivities indicate the spatial arrangement of the imino protons in the secondary structure. The NOE walks are color-coded to the stems in the secondary structure. The 3′ inhomogeneity of the molecule, which is caused by the presence of the N and N+1 species, splits the chemical shifts of imino protons of G131, G191, and U190. Peaks G131* and G191* are from the N+1 impurity molecule, a 57-mer. The peak doubling stops at G134 and does not affect the rest of the molecule.

proton peaks of the 1D spectrum (Fig. 1*b*, *Upper*), and each cross peak connects two diagonal peaks corresponding to protons within 5 Å of each other. Each Watson–Crick G·C and A·U base pair has one imino proton involved in hydrogen bonding; each G·U pair has two imino protons. The imino protons of neighboring base pairs are close enough to give NOE crosspeaks in a 2D spectrum; the two imino protons in a G·U pair give an especially strong cross peak. Different exchange rates of different protons also affect the diagonal and cross peak volumes, but imino-imino NOE crosspeaks between neighboring base pairs were clear. NOEs from the adenine H2 (AH2) of an A·U pair to its U imino proton and to imino protons of neighboring pairs were also useful. The NOE connectivity walks on the 2D spectrum established the assignments and the secondary structure of the RNA as shown in Fig. 1*a*.

The four continuous NOE walks (colored differently) correspond to four stem regions of the secondary structure as shown in Fig. 1*a*. Four U·A pairs were identified by the characteristic crosspeaks between U imino proton and AH2. AH2 protons of these four U·A pairs all have NOEs to the imino protons of flanking base pairs. Four G·U wobble pairs were identified by the intense NOE crosspeaks between their imino protons. The imino protons of all four G·U pairs show NOEs to those of neighboring base pairs. Over 80% of the aromatic H8/H6/H5/H2 and sugar H1′/H2′ region has been assigned for P5abc. Extensive interstrand and internucleotide NOE networks are consistent with the secondary structure shown in Fig. 1*a* and the assignments shown in Fig. 1*b*.

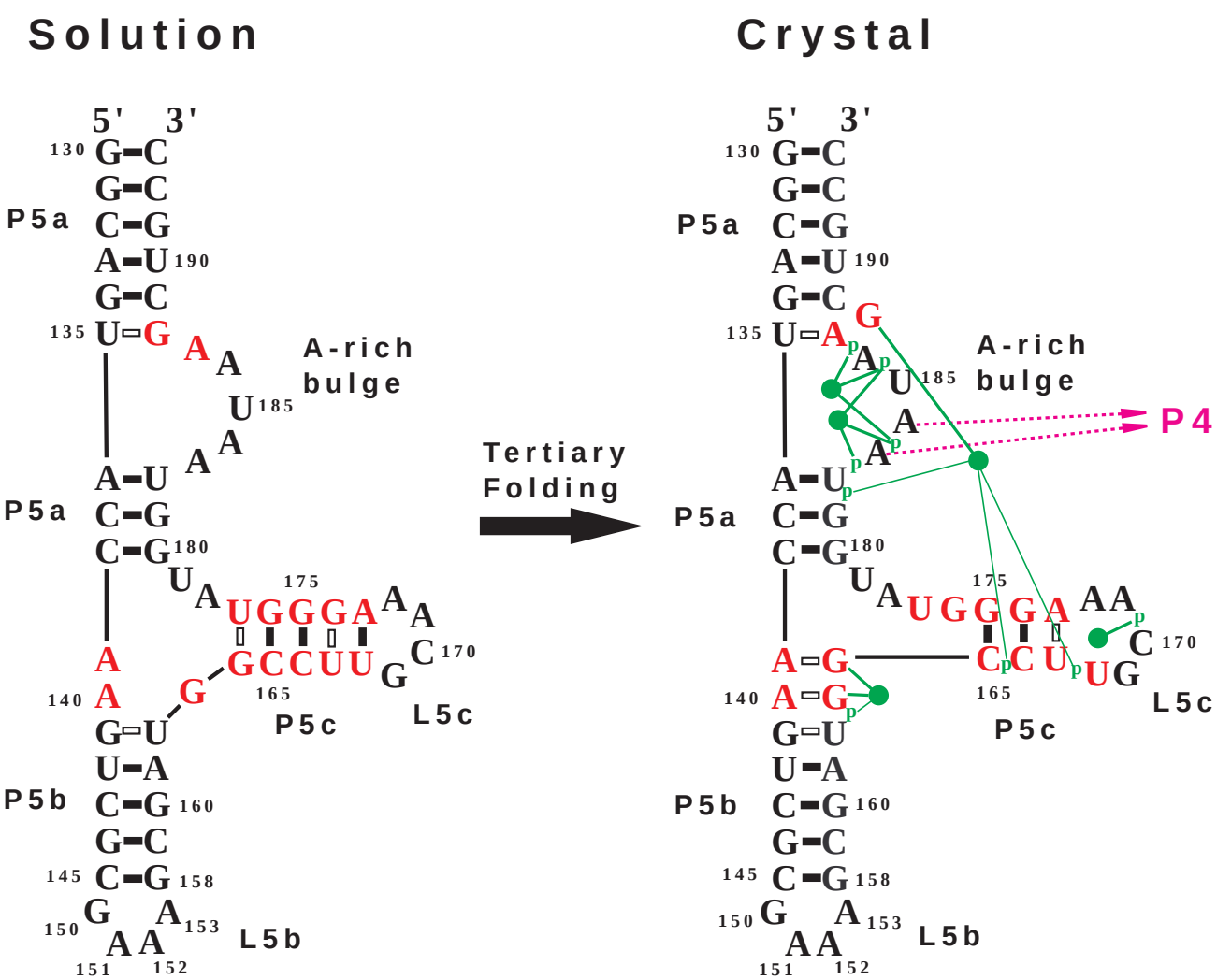

FIG. 2. The secondary structures determined by NMR in solution and by x-ray diffraction in a crystal are compared. Nucleotides that change their base pairing are in red. The solution structure represents the unfolded state, whereas the crystal structure represents the folded state with tertiary interactions. Each solid bar denotes a Watson–Crick base pair, and each hollow bar denotes a non-Watson–Crick base pair. The tertiary interactions seen in the crystal (10) include binding of A183 and A184 to the minor groove of P4 (shown as purple arrows). The green disks represent five magnesium ions identified in the crystal (9, 10) that form direct hydrogen bonds (thick green line) and water-mediated hydrogen bonds (thin green lines) with phosphate oxygens (indicated by p) and guanine bases. The tertiary folding causes significant secondary structure rearrangements, including the loss of three G·U base pairs, the loss of a GNRA tetraloop, the formation of a single base bulge, and the addition of two G·A base pairs.

To further confirm the assignments, three fragments of P5abc, a 27-nt P5a, an 18-nt P5b, and an 18-nt P5c, were synthesized. The P5a fragment includes P5a and the A-rich bulge with the C138·G180 base pair closed by the stable tetraloop UUCG. The P5b fragment contains stem-loop P5b-L5b with two G·C pairs attached to G141·U162. The P5c fragment contains stem-loop P5c-L5c with two G·C pairs attached to G164·U177. The NOE walks of P5abc match well with those in the three fragments. The chemical shift differences between P5abc and the three fragments are very small except at G180, G141, U162, G164, and U177, where P5abc differs significantly from the fragments. These results confirm the chemical shift assignments of P5abc and indicate that the isolated P5a, P5b, and P5c regions have the same secondary structures as when they are in the P5abc subdomain.

Folding P5abc. Many different ionic conditions with different heating and cooling protocols were used to fold P5abc; the extent of folding is very sensitive to RNA concentration, Mg^{2+} concentration, and annealing protocol. Fig. 3 shows the Mg-induced folding of 0.4 mM of P5abc in 10 mM sodium phosphate and 0.05 mM EDTA (pH 6.4) at 20°C. After each increment of Mg^{2+}, the sample was heated at 95°C for 0.5 min and cooled to room temperature. The amount of folding increases with Mg^{2+} concentration and reaches ≈80% at ≥30 mM Mg^{2+}. Many different annealing, titration, and dialysis protocols as well as combinations of RNA and Mg^{2+} concentrations were tried, but a small amount of unfolded species was always observed.

As shown in Fig. 3*d*, when 0.4 mM P5abc is maximally folded, the $[Mg^{2+}]/[P5abc]$ ratio is ≈80:1. However, when the P5abc concentration was increased to 2.5 mM, it showed no folding with the Mg^{2+} concentration up to 55 mM. In this case, the $[Mg^{2+}]/[P5abc]$ ratio is ≈22:1 (= 55/2.5) lower than the 25:1 ratio shown in Fig. 3*b*. Both the $[Mg^{2+}]/[P5abc]$ ratio and the free concentrations of divalent and monovalent ions are obviously important for folding the RNA. This observation is supported by dialysis experiments. When 0.5–3 mM of P5abc was dialyzed against 1–20 mM Mg^{2+}, the P5abc was maximally folded. The folded P5abc (Fig. 3*d*) was unfolded by chelating the Mg^{2+} with EDTA. The 40-mM concentration of EDTA needed to completely unfold the RNA was ≈1.3 times the total Mg^{2+} concentration of 30 mM.

RESULTS

Secondary Structure of P5abc. The secondary structure of the 56-nt P5abc subdomain (Fig. 1*a*) in 10 mM Na^{+} was

determined unambiguously from the imino proton NMR spectrum. The imino protons from guanine and uracil that are base paired, or otherwise prevented from rapid exchange with the solvent, are observable. The 1D spectrum is well resolved, and the 2D NOESY provides assignments of the base pairs (Fig. 1*b*). There are three stems (P5a, P5b, and P5c) with four A·U pairs (U resonances of >13.4 ppm), 11 G·C base pairs (however, the fraying end base pair is not seen in the imino spectrum), four G·U pairs (G resonances between 10.8 and 11.5 ppm), and two G·A resonances (G resonances of <10.8 ppm). The stems form a 3-helix junction with a 5-nt bulge (the A-rich bulge) and two GNRA tetraloops (L5b, L5c). The secondary structure is identical with the predicted secondary structure based on the calculated minimum free energy (ref. 20; free energies were calculated with the program RNA MFOLD on website www.ibc.wustl.edu/~zuker/), except that the predicted structure adds an A139·U179 pair at the end of stem P5a. The secondary structure for the A-rich bulge is the same as that found previously for the isolated A-rich bulge in a stem–loop structure (21). However, the secondary structure of the P5abc subdomain is quite different from the secondary structure present in the P4–P6 domain in the crystal (10) (Fig. 2). In the crystal, the A-rich bulge of 5 nt is divided into two bulges of 4 nt and 1 nt (G188) interrupted by a single A·U base pair, and the GCAA tetraloop (L5c) is increased to 5 nt by shifting the base pairing in the P5c stem. The net effect is to change five base pairs in stem P5c to a different set of three base pairs and to add two G·A base pairs to stem P5b. Three G·U base pairs are lost on forming the crystal secondary structure. The calculated free energy of the crystal secondary structure is significantly higher (less stable) than the one for the solution. Presumably, the tertiary interactions present in the *Tetrahymena* intron and in the P4–P6 domain increase the thermodynamic stability of the folded molecule enough to compensate for a secondary structure with a higher free energy.

Mg^{2+}-Induced Folding Changes Secondary Structure. The crystal structure and the phosphorothioate interference experiments reveal the importance of magnesium ions in the folded state (9, 10). Magnesium-induced folding of P5abc was monitored by changes in the imino proton spectrum on adding Mg^{2+} (Fig. 3). There are minor changes in the spectrum at a 10-mM Mg^{2+} concentration (Fig. 3*b*); however, at a 20-mM concentration, a new conformation is evident from the splitting of the U142 imino peak of the U·A base pair in P5b (Fig. 3*c*). The U142 imino peak (14.31 ppm) intensity decreases, and a corresponding new peak (14.00 ppm) appears. The NOEs to the base pairs on either side of the U·A pair show that the top three base pairs (G·U, U·A, and C·G) in stem P5b (Fig. 2) all exist in two distinct environments. The addition of Mg^{2+} to 30 mM produces predominantly the new, folded conformation (Fig. 3*d*). The conformational change near the G·U pair at the end of the P5b stem is consistent with the crystal structure, where two A·G mismatches, A140·G163 and A139·G164, form right above G139·U162; a Mg^{2+} binds at this site. The six imino peaks corresponding to three G·U base pairs (U135·G188, G164·U177, and U167·G174) that are identified by six arrows in Fig. 3 have nearly disappeared in the folded conformation. 2D NOESY experiments do not reveal paired G·U cross peaks in other parts of the spectrum; the three G·U pairs do not exist in the folded conformation. Furthermore, the characteristic resonance (10.67) for the sheared G·A in the L5c tetraloop is absent in the folded conformation. Although the broader peaks in the presence of Mg^{2+} prevent the complete assignment of the imino spectra, all of the changes are consistent with the differences in secondary structure for the RNA in the crystal and Mg^{2+}-free solution (Fig. 2).

The presence of two sets of resonances corresponding to the folded and unfolded species shows that the secondary and tertiary structures are in slow exchange. The difference in chemical shift for the U142 imino proton in the two species plus the slight line broadening means that the exchange rate between conformers is slower than 30 s^{-1}. The slow kinetics are consistent with the number of base pairs that have to be broken before the tertiary structure can form.

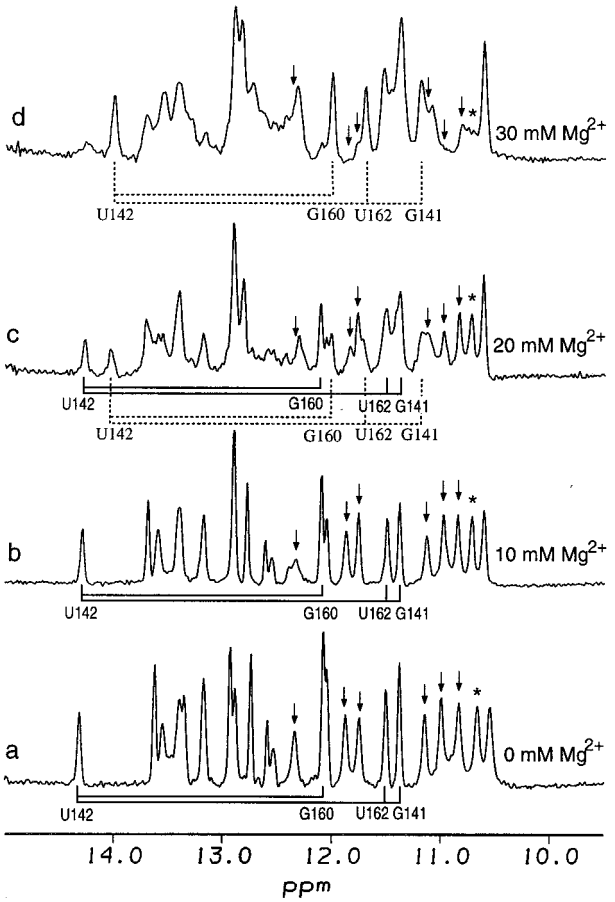

FIG. 3. Mg^{2+}-induced folding monitored by imino proton NMR. Spectra of 0.4 mM of P5abc in 10 mM sodium phosphate and 0.05 mM EDTA (pH 6.4) were measured at 20°C as a function of added $MgCl_2$. The total concentration of Mg^{2+} was 0 mM (*a*), 10 mM (*b*), 20 mM (*c*), and 30 mM (*d*). Solid and dashed lines represent the NOE connectivities as determined by 2D NOESY of 3 bp in stem P5b (G141·U162, U142·A161, and C143·G160) for the unfolded and folded conformations, respectively. With the addition of Mg^{2+}, the four imino proton peaks of these base pairs decrease, and a new set of four imino proton peaks with the same NOE connectivities appear at different chemical shifts. This response is characteristic of a slow exchange between the folded and unfolded conformations. The percentages of folding estimated from the relative intensity of U142 in the folded and unfolded states are ≈50% at 20 mM Mg^{2+} and 80% at 30 mM Mg^{2+}. Six imino proton peaks of three G·U pairs (G188·U135, G164·U177, and G174·U167) disappear during the folding; the peaks are indicated by arrows. NOESY spectra of *c* and *d* show that these six bases no longer form G·U pairs in the folded state. An asterisk indicates the sheared G·A base pair of tetraloop L5c that disappears on folding.

When increasing amounts of EDTA up to a 40-mM concentration were added to the folded P5abc in 30 mM Mg^{2+}, the spectrum gradually changed back to one that was essentially identical with that seen in the absence of magnesium (Fig. 3*a*). An analytical denaturing gel electrophoresis assay of the RNA after folding and unfolding indicated that no degradation had occurred.

A mutant (A186U) of P5abc that has been shown by native gel electrophoresis to not fold (9) in the presence of Mg^{2+} was used as a control for the folded state. The imino proton spectrum of A186U in the absence of Mg^{2+} is identical with that of P5abc wild type, indicating that A186U and P5abc have

identical secondary structures in Na^+. Adding Mg^{2+} to A186U caused little change in its imino proton spectrum, indicating that A186U does not fold into the same tertiary structure as P5abc and does not change its secondary structure in the presence of Mg^{2+}. Native gel electrophoresis experiments on P5abc and the A186U mutant showed identical gel mobilities in the absence of Mg^{2+} but a higher mobility for P5abc in the presence of 5 mM Mg^{2+}, which is in agreement with the results of Cate *et al.* (9). Thus, both NMR and native gel experiments indicate that P5abc folds into a tertiary structure in the presence of Mg^{2+}, whereas A186U does not. The folding behavior in the NMR experiments at millimolar RNA concentrations is similar to that seen at nanomolar concentrations in the gel.

DISCUSSION

The folding of RNA is thought to take place in two steps. In the first step—for example, as the RNA is cooled from a high temperature—base pairs form to produce a secondary structure of stems, mismatches, loops, and bulges. In the second step, the tertiary structure forms with specific loop–loop or loop–bulge interactions or with other long-range RNA–RNA interactions. The simplest assumption, and the one traditionally made, is that the tertiary interactions occur between the unpaired bases of the secondary structure. The folding of tRNA is a prime example (22), as is the formation of pseudoknots from two hairpins (23). In these molecules, the small decrease in free energy on forming the tertiary structure cannot make up any significant increase in free energy caused by disruption of the secondary structure.

We have found a counter example in which the secondary structure of an RNA subdomain in solution changes when the subdomain becomes part of its parent intron and when it is part of a domain of the intron in a crystal. The changes are significant (see Fig. 2). Six base pairs (two G·C, one A·U, and three G·U) are broken, and four new base pairs are formed (two G·C and two non-Watson–Crick A·U). A tetraloop is disrupted, a 1-nt bulge is formed, and two G·A pairs are formed in folding to the tertiary structure. There is a calculated (20) decrease in the thermodynamic stability of the secondary structure by ≈10 kcal (1 kcal = 4.18 kJ) mol^{-1} of free energy at 37°C. This loss in thermodynamic stability is made up by the tertiary interactions. The interactions include the binding of two adenines of the A-rich bulge (A183 and A184) into the minor groove of the P4 helix present in the P4–P6 domain as well as the interaction of the rest of the A-rich bulge (A186, A187, and G188) with the P5b and P5c stems in the subdomain (10). The tertiary folding requires magnesium ions directly coordinated to phosphate oxygens at A171, A183, A184, A186, and A187, and to the bases at G188, G163, and G164 (9, 10). The thermodynamics of secondary structure formation (20) is based on measurements in 1 M NaCl that are similar to those measured in millimolar Mg^{2+}. The effects of magnesium ions are mainly in the formation of the folded tertiary structure, but their contributions to the free energy of folding are not known. The binding of Mg^{2+} will clearly be a sensitive function of the concentration of the Mg^{2+} and of all the other ions in the solution, including the concentration of RNA.

Mg^{2+}-induced folding of the P5abc subdomain monitored by NMR clearly indicates secondary structure rearrangement to a folded conformation consistent with the crystal structure. This observation is contrary to the standard assumption that RNA folds by first forming base-paired helices and loops; the loop regions are then available for the tertiary interactions that hold the helices in their biologically required structure. tRNA was the first example of this folding pathway. The loop conformations and interactions change on tertiary structure formation, but the helices do not. Recent examples include the docking of a tetraloop into a tetraloop receptor (24) and the formation of kissing hairpins (25). Upon RNA tertiary folding, single base pair changes have been observed (21). However, this report demonstrates a major rearrangement in secondary structure in which several adjacent Watson–Crick base pairs are broken and new ones are formed on the folding of an RNA into its tertiary structure. Clearly, it is important to determine both secondary and tertiary structures for other RNAs to ascertain the generality of this finding. Furthermore, to improve prediction of the folded state of an RNA from its sequence, it will be necessary to measure the thermodynamics of tertiary interactions to learn when these interactions can compensate for lost secondary structure base pairs.

We followed the folding of the RNA by measuring its secondary structure in the presence of Na^+ and then observing the changes in base pairing on the addition of Mg^{2+} at constant temperature. This type of isothermal method was used by Sclavi *et al.* (14) to show that the first step in folding a group I intron RNA is formation of the P5abc structure, which nucleates the folding of the intron. We are now using thermal melting and cooling of the RNA in the presence of Mg^{2+} to determine whether the folding path is the same as for an isothermal Mg^{2+} perturbation. Does the same secondary structure present in Na^+ form during the thermal unfolding of the RNA in Mg^{2+}?

The folding mechanisms of RNA are very poorly understood. NMR imino spectra can provide the base-pairing scheme—the secondary structure—for large RNAs (>50 nt). A secondary structure can be determined with much less effort than is necessary to derive an atomic resolution structure from the assignment and analysis of a complete proton NMR spectrum.

We thank Mr. D. Koh for synthesizing the DNA oligonucleotides and Ms. B. Dengler for supervising the laboratory. We also thank Ms. R. Hanna, Dr. J. Cate, and Profs. J. Doudna and D. Wemmer for making many helpful suggestions. This work was supported in part by National Institutes of Health Grant GM 10840, by Department of Energy Grant DE-FG03-86ER60406, and through instrumentation grants from both the Department of Energy (DE-FG05-86ER75281) and the National Science Foundation (DMB 86-09305). M.W. is supported by a Burroughs Welcome Fund Fellowship.

1. Gesteland, R. F. & Atkins, J. F., eds. (1993) *The RNA World* (Cold Spring Harbor Lab. Press, Plainview, NY).
2. Simons, R. W. & Grunberg-Manago, M., eds. (1997) *RNA Structure and Function* (Cold Spring Harbor Lab. Press, Plainview, NY).
3. Jaeger, J. A., Zuker, M. & Turner, D. H. (1990) *Biochemistry* **29,** 10147–10158.
4. Celander, D. W. & Cech, T. R. (1991) *Science* **251,** 401–407.
5. Banerjee, A. R., Jaeger, J. A. & Turner, D. H. (1993) *Biochemistry* **32,** 153–163.
6. Zarrinkar, P. P. & Williamson, J. R. (1996) *Nat. Struct. Biol.* **3,** 432–438.
7. Doherty, E. A. & Doudna, J. A. (1997) *Biochemistry* **36,** 3159–3169.
8. Pyle, A. M. (1993) *Science* **261,** 709–714.
9. Cate, J. H., Hanna, R. L. & Doudna, J. A. (1997) *Nat. Struct. Biol.* **4,** 553–558.
10. Cate, J. H., Gooding, A. R., Podell, E., Zhou, K., Golden, B. L., Kundrot, C. E., Cech, T. R. & Doudna, J. A. (1996) *Science* **273,** 1678–1685.
11. Cate, J. H. & Doudna, J. A. (1996) *Structure (London)* **4,** 1221–1229.
12. Cate, J. H., Gooding, A. R., Podell, E., Zhou, K., Golden, B. L., Szewczak, A. A., Kundrot, C. E., Cech, T. R. & Doudna, J. A. (1996) *Science* **273,** 1696–1699.
13. Downs, W. D. & Cech, T. R. (1996) *RNA* **2,** 718–732.
14. Sclavi, B., Sullivan, M., Chance, M. R., Brenowitz, M. & Woodson, S. A. (1998) *Science* **279,** 1940–1943.
15. Murphy, F. L. & Cech, T. R. (1993) *Biochemistry* **32,** 5219–5300.
16. Milligan, J. F., Groebe, D. R., Witherell, G. W. & Uhlenbeck, O. C. (1987) *Nucleic Acids Res.* **15,** 8783–8798.

17. Wyatt, J. R., Chastain, M. & Puglisi, J. D. (1991) *BioTechniques* **11,** 764–769.
18. Plateau, P. & Gueron, M. (1982) *J. Am. Chem. Soc.* **104,** 7310–7311.
19. Sklenar, V. & Bax, A. (1987) *J. Magn. Reson.* **74,** 469–479.
20. Zuker, M. (1989) *Science* **244,** 48–52.
21. Luebke, K. J., Landry, S. M. & Tinoco, I., Jr. (1997) *Biochemistry* **36,** 10246–10255.
22. Saenger, W. (1984) *Principles of Nucleic Acid Structure* (Springer, New York), pp. 331–349.
23. Wyatt, J. R., Puglisi, J. D. & Tinoco, I., Jr. (1990) *J. Mol. Biol.* **214,** 455–470.
24. Butcher, E. S., Dieckmann, T. & Feigon, J. (1997) *EMBO J.* **16,** 7490–7499.
25. Chang, K.-Y. & Tinoco, I., Jr. (1997) *J. Mol. Biol.* **269,** 52–66.